analytical chemistry

Article

pubs.acs.org/ac

Analysis of *Drosophila* Lipids by Matrix-Assisted Laser Desorption/Ionization Mass Spectrometric Imaging

Ann-Christin Niehoff,[†,‡,§,∥] Hans Kettling,[∥,⊥] Alexander Pirkl,[∥] Yin Ning Chiang,[†] Klaus Dreisewerd,[∥,⊥] and Joanne Y. Yew*[,†,#,$]

[†]Temasek Life Sciences Laboratory, 1 Research Link, Singapore 117604

[‡]NRW Graduate School of Chemistry, University of Münster, Wilhelm-Klemm-Strasse 10, 48149 Münster, Germany

[§]Institute of Inorganic and Analytical Chemistry, University of Münster, Corrensstrasse 30, 48149 Münster, Germany

[∥]Institute for Hygiene, University of Münster, Robert-Koch-Strasse 41, 48149 Münster, Germany

[⊥]Interdisciplinary Center for Clinical Research (IZKF), University of Münster, Domagkstrasse 3, 48149 Münster, Germany

[#]Department of Biological Sciences, National University of Singapore, 14 Science Drive 4, Singapore 117543

[$]Pacific Biosciences Research Center, University of Hawaii at Mānoa, 1993 East-West Road, Honolulu, Hawaii 96822, United States

Supporting Information

ABSTRACT: *Drosophila melanogaster* is a major model organism for numerous lipid-related diseases. While comprehensive lipidomic profiles have been generated for *D. melanogaster*, little information is available on the localization of individual lipid classes and species. Here, we show the use of matrix-assisted laser desorption/ionization mass spectrometric imaging (MALDI-MSI) to profile lipids in *D. melanogaster* tissue sections. The preparation of intact cryosections from whole insects presents a challenge due to the brittle hydrophobic cuticle surrounding the body and heterogeneous tissue types beneath the cuticle. However, the introduction of a novel sucrose infiltration step and gelatin as an embedding media greatly improved the quality of tissue sections. We generated MS image profiles of six major lipid classes: phosphatidylcholine, phosphatidylethanolamine, phosphatidylglycerol, phosphatidylinositol, phosphatidylserine, and triacylglycerides. In addition, signals corresponding to two male-specific sex pheromones were detected in the ejaculatory bulb, a specialized site of pheromone production. MSI performed with 35 μm lateral resolution provided high sensitivity detection of at least 92 different lipid species, based on exact mass. In contrast, MSI with 10 μm lateral resolution enabled the detection of 36 lipid species but allowed lipid profiling of individual organs. The ability to localize lipid classes in intact sections from whole *Drosophila* provides a powerful tool for characterizing the effects of diet, age, stress, and environment on lipid production and distribution.

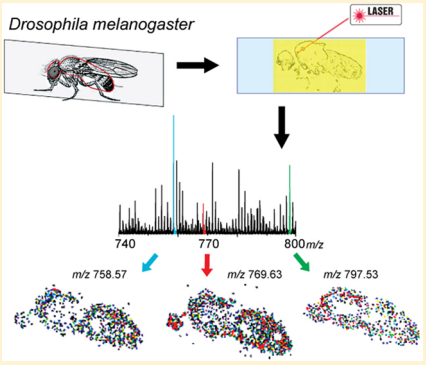

Lipids have fundamental roles for many biological functions such as the maintenance of cell membrane architecture, energy storage, intra- and extra-cellular signaling, and in the case of insect pheromones, chemical communication and social behavior.[1,2] Because of their biological importance, there has been much interest in the development of analytical methods for the detection, structural elucidation, and quantitation of lipids. In particular, matrix-assisted laser desorption/ionization mass spectrometric imaging (MALDI-MSI) has successfully been used to generate chemical maps of lipids from single cells, tissues, and intact animals.[3−6] The ability to distinguish between lipid species while providing spatial localization has been valuable for identifying biomarkers associated with aging[7,8] and disease.[9−13] Here, we demonstrate the first example of lipid imaging of *Drosophila melanogaster*, a major model organism. *D. melanogaster* has been used to elucidate the cellular mechanisms underlying several lipid-related disorders including obesity, Niemann-Pick type C disease, Alzheimer's disease, and Parkinson's disease.[14,15] Several lipidomic analyses of extracts obtained from adult and developing *Drosophila* have been performed.[16−18] However, studies providing spatially refined characterization are limited. While labeling of lipid droplets can be achieved using genetically-encoded fluorescent tags[19] or lipophilic dyes such as Nile Red and BODIPY,[20] both methods offer little specific chemical information. Increasingly, MALDI-MSI has been used to characterize lipids on external cuticles and tissue sections of other insects,[21−26] providing both spatial and structural information.

In this work, we apply MALDI-MSI to *Drosophila* tissue sections. We show for the first time the distribution of six different lipid classes from tissue sections of whole *Drosophila*. In addition, we show localization of signals corresponding to sex-specific pheromones in the male ejaculatory bulb, a

Received: May 8, 2014
Accepted: October 20, 2014
Published: October 20, 2014

 © 2014 American Chemical Society

specialized site of pheromone synthesis.[26−28] Furthermore, we compare the influence of sample preparation procedures, matrix type, ion mode, and lateral resolution on the overall image quality. The classical matrix 2,5-dihydroxybenzoic acid (DHB), commonly used for MSI of lipids, was better suited for the detection of TAGs and PEs. In contrast, dithranol (1,8-dihydroxy-9(10H)-anthracenone), a recently introduced matrix for lipid analysis,[29] was more effective for PI and PE detection, particularly in negative ion mode. Laser spot size greatly influenced signal sensitivity; at 35 μm lateral resolution, more species of lipids were identified within each class. However, while MS imaging with 10 μm lateral resolution resulted in fewer identified lipids, the resolution allowed chemical imaging of lipid distribution in individual organs. Overall, our results demonstrate the efficacy of MALDI-MSI for producing highly detailed maps of lipid distribution within a complex, heterogeneous sample less than 2 mm in length.

EXPERIMENTAL SECTION

Drosophila Husbandry. *Drosophila melanogaster* were raised on autoclaved yeast-sucrose-cornmeal-agar food in a 25 °C room on a 12:12 h light/dark cycle at 60% humidity. Adult flies were isolated at pupal stage and housed with the same sex to prevent exchange of pheromones. Male and female flies were analyzed at 4−5 days old.

Tissue Preparation. Unless otherwise noted, all reagents were obtained from Sigma-Aldrich (St. Louis, MO). For sucrose (purity >99.5%) infiltration, anesthetized flies were placed in a sucrose solution (30% w/v) in distilled water for 1 h at room temperature (RT) prior to embedding in gelatin (10% w/v; no. 4078; Merck, Darmstadt, Germany). Gelatin was heated to 50 °C for 10 min until a homogeneous solution was achieved. A single fly was mounted on the sample holder with a droplet of liquid media, covered with more media, and placed at −25 °C until solidified. Tissue sections 20 μm in thickness were prepared using a cryomicrotome (CryoStar NX70, Thermo Scientific, Bremen, Germany) held at −23 °C. Tissue slices were thaw-mounted on stainless steel (for QSTAR analysis) or standard noncoated histological glass slides (76 mm × 26 mm × 1.2 mm for Synapt G2-S analysis). Between 20 and 25 sections were placed on a single sample plate.

Nile Red Staining. Tissue sections were prepared as for MSI with the addition of an overnight fixation step in 4% paraformaldehyde in 0.1 M phosphate buffered saline (PBS; pH 7.4) at 4 °C prior to sucrose infiltration and a second fixation at 37 °C for 30 min after sectioning. Sections were stained with Nile Red (0.02% (w/v) in 0.1 M PBS) for 40 min at RT.

Matrix Application. 2,5-Dihydroxybenzoic acid (150 mg/mL; DHB) dissolved in 50% methanol or dithranol (8 mg/mL) in chloroform/methanol (2:1, v/v) was applied onto the tissue slices with an airbrush equipped with a 150 μm diameter nozzle (Infinity solo, Harder & Steenbeck, Norderstedt, Germany) using 3 bar of back pressure (N_2). The sample plate was mounted upright 20 cm from the airbrush outlet and 3 s of spraying was alternated with 15 s of air-drying. Between 8 and 10 cycles of matrix application produced a homogeneous layer of DHB crystals approximately 4−8 μm in length and 2−4 μm in width, spaced 3 μm apart or less (Figure S1A,B in the Supporting Information). Dithranol was applied at a sample-airbrush outlet distance of 10 cm using the same time intervals as for DHB. The crystals produced ranged from 0.5−3 μm in length and 2−5 μm in width, spaced less than 5 μm apart (Figure S1C in the Supporting Information). Coated samples were dried at RT for 1 h prior to MS analysis. Glass slides were mounted on a custom-built milled-out sample plate.

Mass Spectrometry. Mass spectra were generated using either a QSTAR Elite (AB Sciex, Concord, Canada) or a Synapt G2-S HDMS (Waters/Micromass, Manchester, U.K.) hybrid orthogonal-extracting time-of-flight (oTOF) mass spectrometer. The QSTAR is equipped with a modified oMALDI2 ion source (AB Sciex; similar to that previously described in ref 30) and an N_2 laser (λ = 337 nm; MNL 106 PD; LTB Lasertechnik, Berlin, Germany) operated at a repetition rate of 40 Hz. The laser beam was coupled into a UV-transmitting glass fiber (CeramOptec; Bonn, Germany) with a 50 μm-core diameter to produce a focal spot size of ∼50 × 100 μm^2 (determined by the size of the ablation craters). MALDI-MSI data were recorded using a step size of 50 μm × 80 μm and a cooling gas pressure of ∼0.8 mbar of N_2 in the ion source. For acquisition of imaging mass spectra, ∼72 laser pulses (of ∼10 μJ pulse energy) were applied per spot corresponding to an acquisition time of 1.8 s. The mass spectra were processed using Analyst software (Analyst QS 2.0, AB Sciex). The mass accuracy was about 10 ppm and the mass resolution (full width at half-maximum, fwhm) > 8000. All mass spectra recorded with the QSTAR were acquired in the positive ion mode.

The MALDI Synapt G2-S HDMS is equipped with a frequency-tripled Nd:YAG laser (λ = 355 nm; Flare PQ UV 1000-30; InnoLight Laser, Kaiserslautern, Germany), operated with a repetition rate of 1 kHz, and a modified ion source, enabling the use of elevated cooling gas pressure and smaller laser spots than provided in the default geometry. Details of laser beam shaping and modifying the focal spot size were previously described.[31] MALDI-MS images were recorded with two effective laser spot sizes of ∼35 μm and ∼10 μm in diameter and using a cooling gas pressure (N_2) of ∼0.8 mbar. For the 35 μm spot, a step size of the sample stage of 50 μm × 50 μm was used. For the ∼10 μm-wide spot, the step size was 11.25 μm × 11.25 μm; 250 laser pulses were applied per pixel. The effective laser spot sizes (area of visible material ablation) were determined by investigating the ablation craters formed in the matrix after the measurements. Measurements with the Synapt were made in both the positive and negative ion modes providing a mass resolution of about 20 000 (fwhm) and a mass accuracy of <10 ppm.

Identification of Lipid Species. Lipid identification was based on comparison between experimental and theoretical m/z values. The composition of the individual fatty acyl moieties cannot be derived from m/z value of the molecular ion alone. To corroborate assignments, tandem MSI measurements were performed on selected lipid species with a collision energy (E_{lab}) of 25 eV using Ar as the collision gas.

Image Processing. Imaging data were processed and visualized using BioMAP software (v 3.8.0.4, Novartis, Basel Switzerland; http://www.maldi-msi.org/). The bin width was set to 0.02 Da and contrast values were selected to encompass the full dynamic range of signal intensity from all the lipid classes, with the exception of the sex pheromones. The latter were analyzed with different minimum and maximum intensity thresholds, due to lower abundances.

RESULTS AND DISCUSSION

Infiltration and Embedding Media for Sample Preparation. Preparation of intact cryosections from whole *Drosophila* presents several challenges. First, each section consists of heterogeneous tissue-types, each of which may

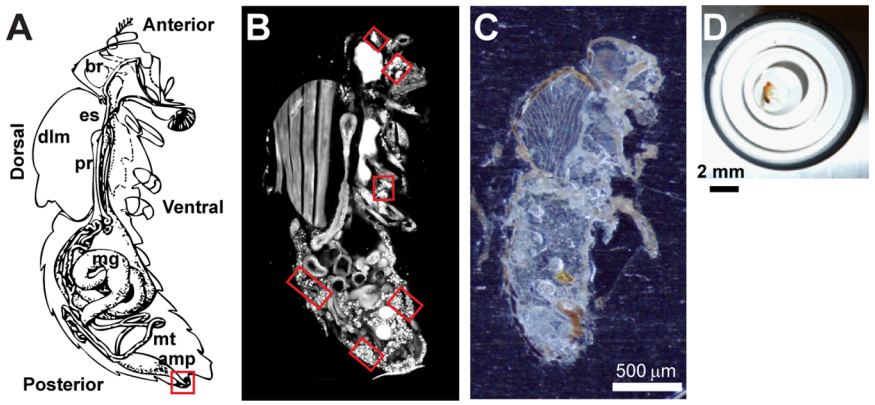

Figure 1. (A) Illustration showing internal organs of *D. melanogaster*, including respiratory system, digestive system, and reproductive organs. Adapted with permission from an image by A. Miller, ref 42. Copyright 1994 Cold Spring Harbor Laboratory Press. The proximate region of the ejaculatory bulb and anogenital region is boxed in red. Labeled anatomical features: brain (br), dorsal longitudinal muscles (dlm), esophagus (es), proventriculus (pr), midgut (mg), Malpighian tubules (mt), and rectal ampulla (amp). (B) Tissue section of a male *Drosophila* stained with Nile Red shows the accumulation of lipid droplets in the fat body and other compartments (boxed in red) underlying the cuticle and surrounding the internal organs. (C) Longitudinal cryosection of a male *D. melanogaster*, mounted on a stainless steel sample plate, prior to matrix application and MSI analysis. (D) Male *Drosophila* embedded in 10% gelatin and mounted on a cryotome sample stage, prior to sectioning.

require different sectioning conditions. Notably, the external cuticle is a hard, waxy surface while internal structures are softer and surrounded by viscous hemolymph and the fat body, a thin layer of fat residing beneath the cuticle (Figure 1A,B). Second, the hydrophobic external cuticle prevents complete coverage by a hydrophilic embedding medium. These problems were ameliorated by the use of a novel infiltration step and gelatin embedding media. Immersion of intact anesthetized flies in a sucrose solution allowed complete coverage by the embedding media and produced a more homogeneous consistency throughout the sample, thus facilitating the production of intact cryosections. One drawback of the infiltration step is that signals corresponding to sucrose and sucrose multimers were detected from about m/z 299 to 877, overlapping with the mass range of interest. However, the signals exhibit a low mass increment and are distinguishable from tissue-specific lipid analytes which have a high mass increment.

Optimization of the embedding media was also crucial to the generation of intact cryosections. Gelatin, which has previously been used to embed the pericardial organ and brain from crab,[32] yielded intact tissue sections and produced no interfering signals (Figure 1C,D). Agarose (1% or 5%) and poly[*N*-(2-hydroxypropyl) methacrylamide] (pHPMA; 15% or 20%)[23] were also tested but the former solidified too rapidly and the latter, in our hands, did not easily produce flat sections. For these reasons, gelatin was used in all MSI experiments presented.

Comparison of Instrumental Parameters. Initial MSI experiments were performed using a QSTAR mass spectrometer with ~50 μm × 80 μm lateral resolution. DHB was used as a matrix for the experiments since it is well-established as a matrix for MSI of lipids. A total of 46 different lipids were identified including phosphatidylcholines (PC), phosphatidylethanolamines (PE), phosphatidylglycerols (PG), triacylglycerides, and male sex pheromones (Figure S2 and Table S2 in the Supporting Information). All of the glycerolipids had been detected from previous lipidomic analyses of *Drosophila* extract.[16,17] There were several limitations with the QSTAR platform. First, phosphatidylserine (PS), one of the more abundant lipid classes, was not detected. Second, the lateral resolution was insufficient to provide fine detail of the internal organs. Third, because of the limited mass accuracy of the instrument, it was not possible to resolve ambiguities in structural assignments. MSI analysis is complicated by the pairing of the same lipid species with different charged ions within the same tissue section. This heterogeneity can generate ion signals that are nearly isobaric with other lipid species and confounds structural assignment based on m/z alone. For example, the mass difference resulting from an exchange of potassium and sodium (15.974 u) is very similar to the mass shift resulting from an addition of oxygen (15.995 u). For these reasons, we cannot exclude the possibility of isobaric species contributing to the ion signal.

To refine analysis of *Drosophila* tissue sections, we performed additional experiments on a Synapt G2-S instrument. The G2-S instrument features a smaller laser spot size (diameter = 35 μm) compared to that of the QSTAR (50 × 80 μm^2), higher resolving power, and improved mass accuracy.[31] With the exception of PSs, which were not detected with the QSTAR, both sets of measurements resulted in the detection of the same lipids and with similar sensitivity using DHB as a matrix (Figure 3). Interestingly, PC molecules with potassium-adducts were more prominent in the QSTAR. This observation probably reflects the higher collisional cooling efficiency achieved with the QSTAR[33] enabling the detection of weakly bound molecule-ion complexes. Other differences in ion signal distributions found between Synapt and QSTAR measurements are more likely due to the use of tissue from different locations within the fly and variation between animals.

To improve the resolution and enhance the detection of other lipid classes on the Synapt, three further experimental parameters were investigated: laser spot size, matrix type, and ion mode. Increasing the lateral resolution to ~10 μm (as described in ref 31) significantly enhanced the delineation of fine features in the fly section such as the ovaries and different sections of the gut (Figure 4B). In general, however, fewer lipid species were detected since signal intensity was lower overall with increased lateral resolution. With respect to matrix, we compared DHB to dithranol. Dithranol was selected because of its effectiveness in both the negative and positive ion mode.[29,31] In addition, dithranol is soluble in chloroform/methanol, a common solvent system for lipid extraction that, upon airbrush-

spraying, evaporates rapidly and forms homogeneous layers of micrometer-sized matrix crystals. This latter feature is necessary for facilitating MS analysis with high lateral resolution. Our results indicate that the use of DHB improved detection of PEs and TAGs in the positive ion mode whereas PGs were better detected with dithranol. Lastly, in negative ion mode, experiments using dithranol identified 11 species of PI, a lipid class that was not found in other conditions (Table S3 in the Supporting Information). However, for most other lipid species, higher ion abundances are detected in the positive ion mode. The individual profiles of the detected lipids are discussed in detail below.

Detected Lipid Classes. Seven distinct lipid classes were detected by MALDI-MSI in positive or negative ion mode. A list of all identified lipid species (based on exact mass measurements and predicted elemental composition) is provided in Tables S1−S3 in the Supporting Information.

Phosphatidylcholine. PCs are among the most abundant phospholipids in animals and are major components of the outer leaflet of biological membranes.[34] Ion signals corresponding to PCs ranging in overall fatty acyl chain length from 28−38 carbon atoms were detected with high intensity by MALDI-MSI from both male (Figure 2) and female tissues (Figure 3) prepared with either DHB or dithranol. A total of 15 species of PCs were detected at ∼35 μm resolution whereas only 11 species were identified using a spot size of ∼10 μm in diameter (Table S1 in the Supporting Information). The influence of laser beam spot size on signal intensity is consistent with the results of previous studies.[31,35,36] However, the higher lateral resolution allowed for fine delineation of internal organs such as the ovaries and the midgut region (Figure 4). PCs are particularly enriched in regions surrounding the brain tissue, abdomen, germ cells, and ventral subcuticular region (Figures 3B and 4A). Fragment ions resulting from the loss of $N(CH_3)_3$ also were observed, primarily with the 35 μm spot (Tables S1 and S2 in the Supporting Information). To confirm structural identification, MS imaging in the tandem MS mode was performed on a signal corresponding to protonated PC (34:2) (m/z 758.57). The distribution of the characteristic fragment signal at m/z 184.07 (indicative of the phosphorylcholine headgroup; Figure 4C) corresponds well to that of the precursor ion (Figure 4D). Neutral loss signals that could be used to deduce the fatty acyl composition were not detected, due to the relatively low abundance of the precursor, and therefore only the overall carbon numbers and degree of unsaturation can be determined. Overall, ion abundances recorded using dithranol were lower compared to those obtained from DHB (Figure 4) though the same PC species were detected with each matrix.

Phosphatidylserine. Approximately 2−10% of the lipids in mammalian cells are estimated to consist of phosphatidylserines.[1] The PSs are ubiquitous in many tissues and are particularly enriched in the brain.[1] Numerous PS species were identified from both males and females using ∼35 μm resolution conditions, with overall carbon lengths ranging from 30−36 (Table S1 in the Supporting Information). Ion signals for several unsaturated PS species (30:2, 32:2, 34:2) were enriched in the posterior regions of males and females, in the region of the ovaries and testes (Figure 3C). However, with ∼10 μm resolution, no signals corresponding to PS were detected, neither in positive nor negative ion mode using either DHB or dithranol.

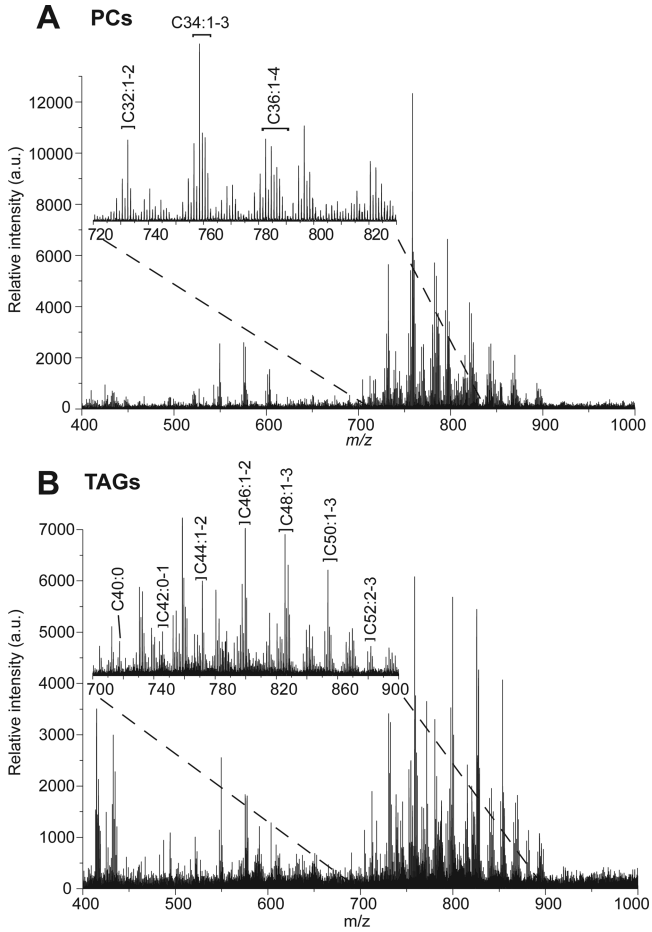

Figure 2. Representative positive ion mode mass spectra corresponding to (A) phosphatidylcholine and (B) triacylglycerides. Mass spectra were acquired from a male *D. melanogaster* cryosection using the Synapt G2-S mass spectrometer and DHB as a matrix. Spectra were recorded from two single irradiated 35 μm-wide pixels, enriched with PCs and TAGs, respectively. Major signals of protonated PC and sodiated TAG pseudomolecular ions are shown in the insets. Signals corresponding to lipids from each class are labeled with the number of carbon atoms followed by the number of double bonds. See Table S1 in the Supporting Information for observed and theoretical m/z values and the putative identity of other detected ion species.

Phosphatidylethanolamine. PEs are commonly distributed in biological tissues on the inner leaflet of the plasma membrane.[34] Different PE species showed distinct patterns of spatial distribution: some species were highly concentrated in a single region such as the ventral thorax (36:3) or germ cells (36:4) while other PEs (36:5) were more evenly distributed throughout the section (Figures 3D and 4). The signal intensity of PEs was overall lower than those for PCs or PSs when comparing MS images acquired under the same conditions (∼35 μm, DHB) and rendered using the same image gain settings (Figure 3D). In contrast to sections coated with DHB, use of dithranol showed overall poor sensitivity for PEs in positive ion mode, with only 2 species detected (Figure 4C). However, in negative ion mode, seven different species of PEs were found using dithranol and signal intensity was higher overall (Figure 4F; Table S3 in the Supporting Information).

Phosphatidylglycerol. PGs are major constituents of bacterial, plant, and animal cell membranes.[37] PGs are commonly detected in the negative ion mode due to the

dx.doi.org/10.1021/ac503171f | *Anal. Chem.* 2014, 86, 11086−11092

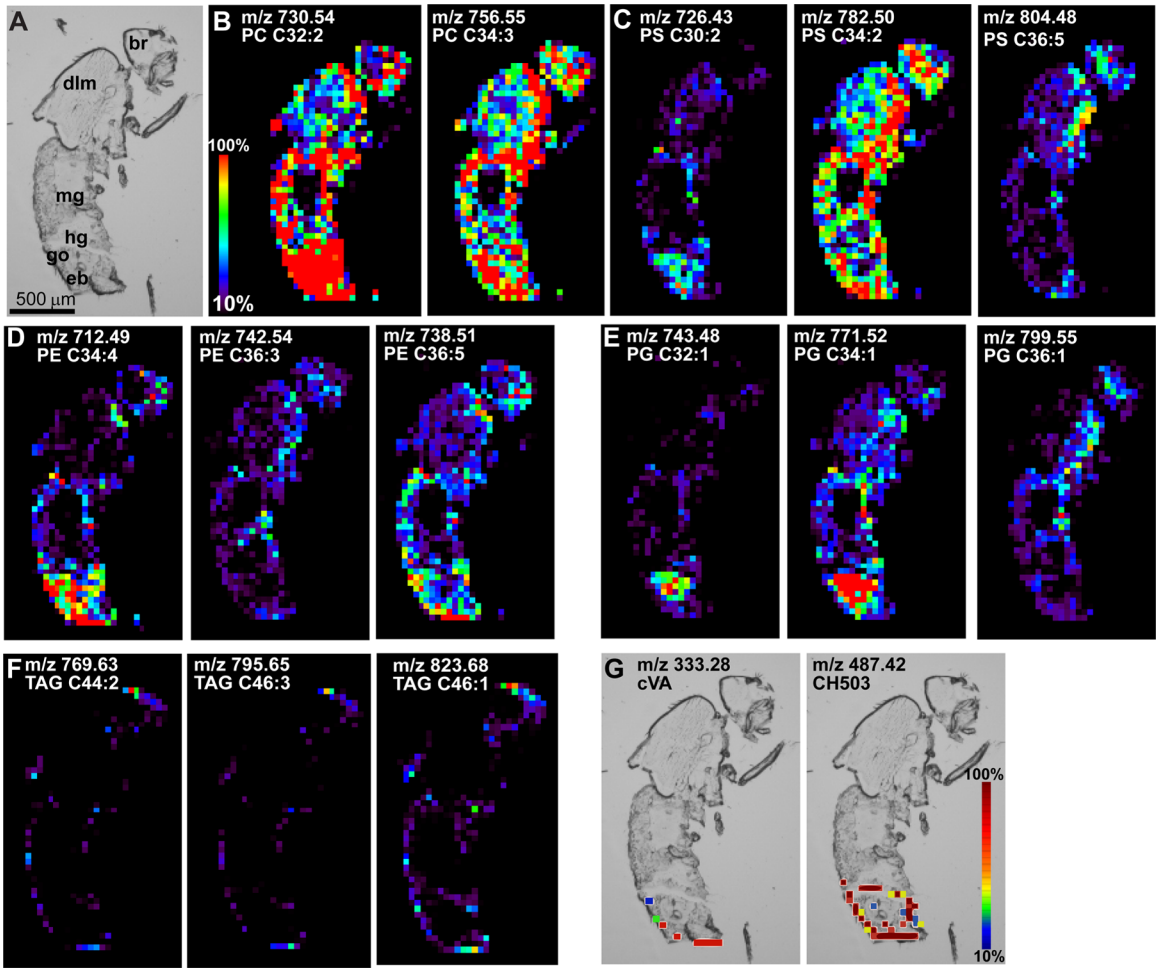

Figure 3. MALDI-MS ion images acquired with 35 μm lateral resolution from a longitudinal section of male *Drosophila*. An optical image of the section prior to matrix application is shown in part A. Labeled anatomical features: brain (br), dorsal longitudinal muscles (dlm), midgut (mg), hindgut (hg), gonads (go), and ejaculatory bulb (eb). MS images of distinct lipid species (as indicated on the top of each image) for six different classes: (B) PC, (C) PS, (D) PE, (E) PG, (F) TAG, and (G) male sex pheromones cVA and CH503. MALDI-MS images were obtained with the Synapt G2-S mass spectrometer using the positive ion mode and DHB as a matrix. The intensity scales used for visualizing the glycerolipid and pheromone distribution are shown in parts B and G, respectively.

presence of a negatively charged headgroup. However, sodium adducts of PGs are also detected in the positive ion mode. Different PG species showed distinct spatial patterns, either concentrating in the thorax and head (36:1), germ cell layers (32:1), or more ubiquitously throughout the section (34:1; Figure 3E). Tissues prepared with dithranol generally showed higher signal intensity for PGs (Figure 4C). Four different species identified with dithranol in the positive ion mode that were not observed with DHB at ~10 μm resolution.

Triacylglycerides. In adult flies, TAGs are stored in lipid droplets that accumulate in the fat body.[38] Seventeen species of TAGs were detected in male and female flies, ranging in overall fatty acyl chain length from C40 to C52 (Figure 2 and Figure S2 in the Supporting Information). The TAGs were localized primarily to the external viscera and enriched in the region underlying the external cuticle on the ventral abdomen, consistent with previous localization studies.[39] With ~35 μm resolution and using DHB as a matrix, the TAG species detected displayed a similar spatial pattern (Figure 3F, Figure S2 in the Supporting Information). However, the 10 μm resolution settings revealed the enrichment of some TAG species in distinct subcuticular layers (Figure 4B). Notably, no TAGs were detected using dithranol in either positive or negative ion mode.

Phosphatidylinositol. PIs are a common cell membrane component found in most tissue-types but are particularly enriched in the brain.[37] Nine species of PIs were detected only in negative ion mode using dithranol as a matrix and showed significant variation in spatial expression with fatty acyl composition. For example, signals for PI (36:3) were highly abundant throughout the entire section, particularly in the regions surrounding the mid- and hindgut and in the brain. In contrast, PI (36:5) was localized mainly in neural tissue.

Sex Pheromones. *D. melanogaster* males produce two known sex pheromones in the ejaculatory bulb: cis-vaccenyl acetate (cVA; (*Z*)-11-octadecen-1-yl acetate) and CH503 ((3*R*,11*Z*,19*Z*)-3-acetoxy-11,19-octacosadien-1-ol).[27,28] The lipid pheromones are secreted to the external anogenital region, transferred to females during mating, and inhibit sexual attraction from other males. Females have not been shown to produce these molecules. Both cVA and CH503 were detected close to the posterior end of the fly body using DHB and ~35 μm resolution (Figure 3G). This observation is consistent with previous studies which identified the sex pheromones from the external anogenital region of the male fly[26−28] or from the

dx.doi.org/10.1021/ac503171f | *Anal. Chem.* 2014, 86, 11086−11092

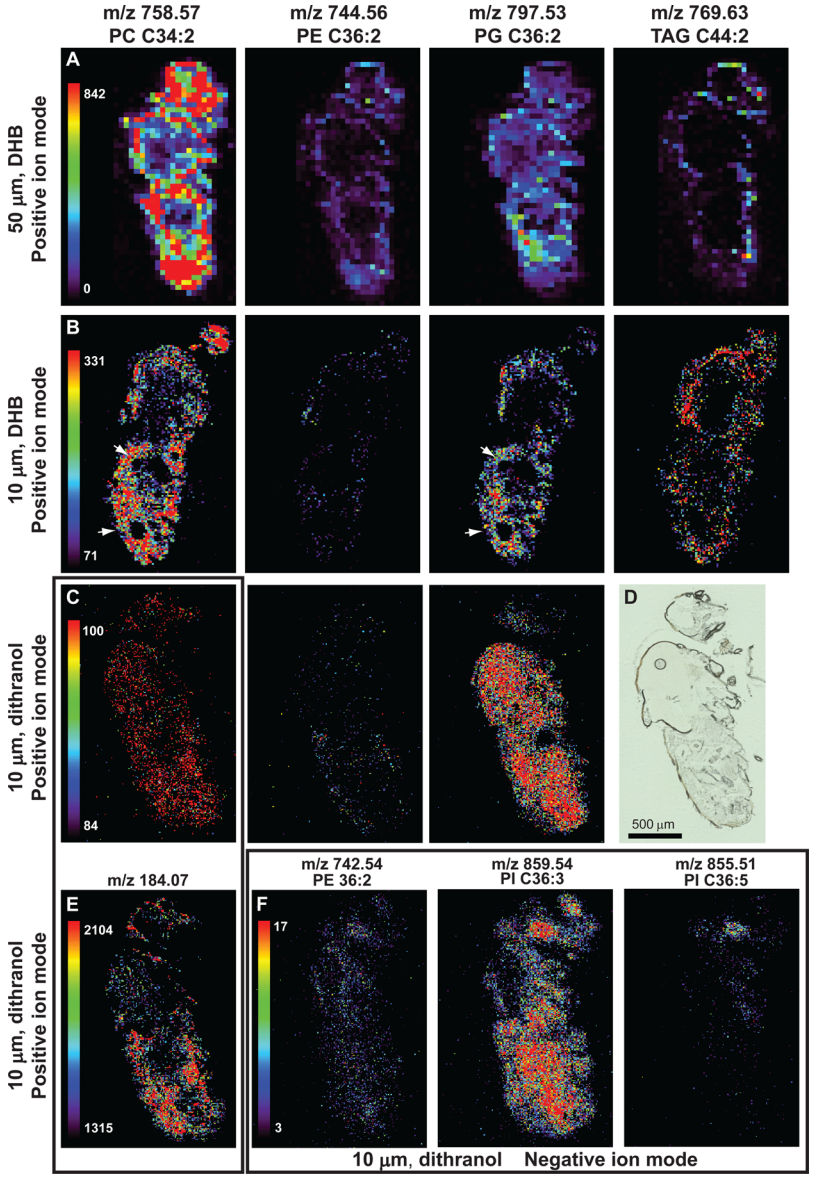

Figure 4. MALDI-MS ion images acquired from longitudinal sections of female *Drosophila*. (A) MS images of PCs, PEs, PGs, and TAGs were obtained with 35 μm resolution measured using DHB as a matrix. Images with 10 μm resolution were acquired using both (B) DHB and (C) dithranol. The higher lateral resolution enabled fine delineation of the midgut and ovaries (B, arrows). (D) Optical image of the female fly section used for dithranol experiments. (E) The tandem MS image of PC (34:2) (shown in part C) was acquired in positive ion mode with a mass selection window of m/z 758.57 ± 1.5. The spatial distribution revealed for the characteristic phosphatidylcholine headgroup fragment (m/z 184.07) corresponds well to that of the parent ion at m/z 758.57. (F) MS images of PE and PIs recorded in negative ion mode with 10 μm resolution using dithranol as a matrix. The intensity scales used for visualizing glycerolipid distribution are placed in the left column and part F.

dissected ejaculatory bulb tissue.[40] This report is the first *in situ* localization of the male sex pheromones to the site of production. The roughly circular shape of the CH503-positive region corresponds well with the globular shape of the ejaculatory bulb and is consistent with the position of the bulb close to the male anogenital region. The high volatility of cVA combined with the vacuum conditions in the ion source may contribute to the low signal intensity. Modifying the source pressure conditions or use of a cooling stage[41] may help to increase sensitivity for low molecular weight volatile molecules such as pheromones.

CONCLUSIONS

We have developed a method for MSI analysis of *Drosophila* tissue sections. The introduction of a sucrose infiltration media and the use of a gelatin embedding media enabled production of intact cryosections from whole insects. Chemical maps of six major glycerolipid classes were produced in addition to the first MALDI-MS image of sex pheromones from the ejaculatory bulb of male *Drosophila*. Increasing the lateral resolution from ~35 μm to ~10 μm resulted in decreased sensitivity for PE, PS, and PG ions and fewer lipid species were identified. However, the improved spatial resolution is more informative for small samples such as *Drosophila*, particularly with respect to the lipid composition of internal organs. Moreover, the matrix type influenced the subset of lipids that were detected: DHB was better suited for the detection of PEs and TAGs while PGs were more easily detected with dithranol. Finally, the use of the negative ion mode allowed improved detection of PEs and PIs. For future applications, the infiltration step used for preparing

dx.doi.org/10.1021/ac503171f | *Anal. Chem.* 2014, 86, 11086−11092

fly tissue sections could potentially be applied to other sample types such as small organisms or tissues with heterogeneous composition. In addition, the ability to detect semiquantitative changes in lipid distribution and abundance will facilitate screening of mutant fly lines for lipid-related defects, particularly when coupled with tandem MS.

■ ASSOCIATED CONTENT

Supporting Information

Additional information as noted in text. This material is available free of charge via the Internet at http://pubs.acs.org.

■ AUTHOR INFORMATION

Corresponding Author

*Phone: +65-6872-8419. E-mail: joanne@tll.org.sg.

Notes

The authors declare no competing financial interest.

■ ACKNOWLEDGMENTS

We thank W. C. Ng and J. S. R. Chin for helpful suggestions on the cryosection protocol, L. Guyonvarch for creating the table of contents graphic, M. Strohalm for the kind gift of pHPMA, and Waters for technical assistance. This work was supported by the Singapore National Research Foundation (Grant NRF-RF2010-06 to J.Y.Y.), the Alexander von Humboldt Foundation (J.Y.Y.), the German Science Foundation (Grants DR 416/9-1, DR 416/10-1 to K.D.), and the Interdisciplinary Center for Clinical Research (IZKF) Münster (Grant Z03 to K.D.). A.C.N. was supported by the Division of Analytical Chemistry of the Germany Chemical Society (GDCh) and the NRW Graduate School of Chemistry (Münster, Germany).

■ REFERENCES

(1) Vance, J. E.; Steenbergen, R. *Prog. Lipid Res.* **2005**, *44*, 207−234.

(2) Wyatt, T. D. In *Pheromones and Animal Behavior: Communication by Smell and Taste*; Cambridge University Press: Cambridge, U.K., 2003.

(3) Chaurand, P.; Cornett, D. S.; Angel, P. M.; Caprioli, R. M. *Mol. Cell. Proteomics* **2010**, *10*, O110.004259.

(4) Watrous, J. D.; Dorrestein, P. C. *Nat. Rev. Microbiol.* **2011**, *9*, 683−694.

(5) Römpp, A.; Spengler, B. *Histochem. Cell Biol.* **2013**, *139*, 759−783.

(6) Nelson, K. A.; Daniels, G. J.; Fournie, J. W.; Hemmer, M. J. *J. Biomol. Technol.* **2013**, *24*, 119−127.

(7) Amaya, K. R.; Sweedler, J. V.; Clayton, D. F. *J. Neurochem.* **2011**, *118*, 499−511.

(8) Ellis, S. R.; Wu, C.; Deeley, J. M.; Zhu, X.; Truscott, R. J.; in het Panhuis, M.; Cooks, R. G.; Mitchell, T. W.; Blanksby, S. J. *J. Am. Soc. Mass Spectrom.* **2010**, *21*, 2095−2104.

(9) Ruh, H.; Salonikios, T.; Fuchser, J.; Schwartz, M.; Sticht, C.; Hochheim, C.; Wirnitzer, B.; Gretz, N.; Hopf, C. *J. Lipid Res.* **2013**, *54*, 2785−2794.

(10) Ishikawa, S.; Tateya, I.; Hayasaka, T.; Masaki, N.; Takizawa, Y.; Ohno, S.; Kojima, T.; Kitani, Y.; Kitamura, M.; Hirano, S.; Setou, M.; Ito, J. *PLoS One* **2012**, *7*, e48873.

(11) Liu, Y.; Chen, Y.; Momin, A.; Shaner, R.; Wang, E.; Bowen, N. J.; Matyunina, L. V.; Walker, L. D.; McDonald, J. F.; Sullards, M. C.; Merrill, A. H., Jr. *Mol. Cancer* **2010**, *9*, 186.

(12) Willems, S. M.; van Remoortere, A.; van Zeijl, R.; Deelder, A. M.; McDonnell, L. A.; Hogendoorn, P. C. *J. Pathol.* **2010**, *222*, 400−409.

(13) Thomas, A.; Patterson, N. H.; Marcinkiewicz, M. M.; Lazaris, A.; Metrakos, P.; Chaurand, P. *Anal. Chem.* **2013**, *85*, 2860−2866.

(14) Liu, Z.; Huang, X. *Acta. Biochim. Biophys. Sin. (Shanghai)* **2012**, *45*, 44−50.

(15) Kraut, R. *J. Neurochem.* **2011**, *116*, 764−778.

(16) Guan, X. L.; Cestra, G.; Shui, G.; Kuhrs, A.; Schittenhelm, R. B.; Hafen, E.; van der Goot, F. G.; Robinett, C. C.; Gatti, M.; Gonzalez-Gaitan, M.; Wenk, M. R. *Dev. Cell* **2012**, *24*, 98−111.

(17) Carvalho, M.; Sampaio, J. L.; Palm, W.; Brankatschk, M.; Eaton, S.; Shevchenko, A. *Mol. Syst. Biol.* **2012**, *8*, 600.

(18) Scheitz, C. J.; Guo, Y.; Early, A. M.; Harshman, L. G.; Clark, A. G. *PLoS One* **2013**, *8*, e72726.

(19) Tian, Y.; Bi, J.; Shui, G.; Liu, Z.; Xiang, Y.; Liu, Y.; Wenk, M. R.; Yang, H.; Huang, X. *PLoS Genet.* **2011**, *7*, e1001364.

(20) Kühnlein, R. P. *Prog. Lipid Res.* **2011**, *50*, 348−356.

(21) Bhandari, D. R.; Römpp, A.; Spengler, B. Presented at the *47th Annual Conference of the German Society for Mass Spectrometry (DGMS)*, Frankfurt am Main, Germany, March 3−5, 2014.

(22) Khalilih, S. M.; Römpp, A.; Prezel, J.; Becker, K.; Spengler, B. Presented at the *47th Annual Conference of the German Society for Mass Spectrometry (DGMS)*, Frankfurt am Main, Germany, March 3−5, 2014.

(23) Strohalm, M.; Strohalm, J.; Kaftan, F.; Krásný, L.; Volný, M.; Novák, P.; Ulbrich, K.; Havlíček, V. *Anal. Chem.* **2011**, *83*, 5458−5462.

(24) Kaspar, S.; Peukert, M.; Svatoš, A.; Matros, A.; Mock, H. P. *Proteomics* **2014**, *11*, 1840−1850.

(25) Vrkoslav, V.; Muck, A.; Cvačka, J.; Svatoš, A. *J. Am. Soc. Mass Spectrom.* **2009**, *21*, 220−231.

(26) Kaftan, F.; Vrkoslav, V.; Kynast, P.; Kulkarni, P.; Böcker, S.; Cvačka, J.; Knaden, M.; Svatoš, A. *J. Mass Spectrom.* **2014**, *49*, 223−232.

(27) Yew, J. Y.; Dreisewerd, K.; Luftmann, H.; Müthing, J.; Pohlentz, G.; Kravitz, E. A. *Curr. Biol.* **2009**, *19*, 1245−1254.

(28) Guiraudie-Capraz, G.; Pho, D. B.; Jallon, J. M. *Integr. Zool.* **2007**, *2*, 89−99.

(29) Le, C. H.; Han, J.; Borchers, C. H. *Anal. Chem.* **2014**, *84*, 8391−8398.

(30) Yew, J. Y.; Soltwisch, J.; Pirkl, A.; Dreisewerd, K. *J. Am. Soc. Mass Spectrom.* **2011**, *22*, 1273−1284.

(31) Kettling, H.; Vens-Cappell, S.; Soltwisch, J.; Pirkl, A.; Haier, J.; Müthing, J.; Dreisewerd, K. *Anal. Chem.* **2014**, *86*, 7798−7805.

(32) DeKeyser, S. S.; Kutz-Naber, K. K.; Schmidt, J. J.; Barrett-Wilt, G. A.; Li, L. *J. Proteome Res.* **2007**, *6*, 1782−1791.

(33) Pirkl, A.; Meier, M.; Popkova, Y.; Letzel, M.; Schnapp, A.; Schiller, J.; Dreisewerd, K. *Anal. Chem.* **2014**, *86*, 10763−10771.

(34) Skipski, V. P.; Peterson, R. F.; Barclay, M. *Biochem. J.* **1964**, *90*, 374−378.

(35) Dreisewerd, K. *Chem. Rev.* **2003**, *103*, 395−426.

(36) Dreisewerd, K.; Schürenberg, M.; Karas, M.; Hillenkamp, F. *Int. J. Mass Spectrom. Ion Processes* **1995**, *141*, 127−148.

(37) Christie, W. W. In *The AOCS Lipid Library*; Harwood, J. L.; Weselake, R. J., Ed.; American Oil Chemists' Society: Urbana, IL, 2011.

(38) Kühnlein, R. P. *J. Lipid Res.* **2012**, *53*, 1430−1436.

(39) Snodgrass, R. In *Principles of Insect Morphology*; Cornell University Press: Ithaca, NY, 1935.

(40) Chin, J. S.; Ellis, S. R.; Pham, H. T.; Blanksby, S. J.; Mori, K.; Koh, Q. L.; Etges, W. J.; Yew, J. Y. *Elife* **2014**, *3*, e01751.

(41) Pirkl, A.; Soltwisch, J.; Draude, F.; Dreisewerd, K. *Anal. Chem.* **2014**, *84*, 5669−5676.

(42) Demerec, M. In *Biology of Drosophila*; Cold Spring Harbor Laboratory Press: Cold Spring Harbor, NY, 1994.